International Journal of Nanomedicine

Dovepress
open access to scientific and medical research

Open Access Full Text Article

ORIGINAL RESEARCH

Induction of apoptosis in cancer cells by NiZn ferrite nanoparticles through mitochondrial cytochrome C release

This article was published in the following Dove Press journal:
International Journal of Nanomedicine
29 October 2013
Number of times this article has been viewed

Mothanna Sadiq Al-Qubaisi[1]
Abdullah Rasedee[1,2]
Moayad Husein Flaifel[3]
Sahrim Hj Ahmad[3]
Samer Hussein-Al-Ali[1]
Mohd Zobir Hussein[4]
Zulkarnain Zainal[4]
Fatah H Alhassan[4]
Yun H Taufiq-Yap[4]
Eltayeb EM Eid[5]
Ismail Adam Arbab[1]
Bandar A Al-Asbahi[3]
Thomas J Webster[6,7]
Mohamed Ezzat El Zowalaty[1,8,9]

[1]Institute of Bioscience, [2]Faculty of Veterinary Medicine, Universiti Putra Malaysia, [3]Faculty of Science and Technology, Universiti Kebangsaan Malaysia, [4]Faculty of Science, Universiti Putra Malaysia, Selangor, Malaysia; [5]College of Pharmacy, Qassim University, Buraidah, Saudi Arabia; [6]Department of Chemical Engineering and Program in Bioengineering, Northeastern University, Boston, MA, USA; [7]Center of Excellence for Advanced Materials Research, King Abdulaziz University, Jeddah, Saudi Arabia; [8]Faculty of Pharmacy, Zagazig University, Zagazig, Egypt; [9]Faculty of Public Health and Tropical Medicine, Jazan University, Jazan, Saudi Arabia

Correspondence: Abdullah Rasedee
Faculty of Veterinary Medicine, Universiti Putra Malaysia, 43400 UPM Serdang, Selangor, Malaysia
Tel +60 389 463 455
Fax +60 389 461 971
Email rasedee@vet.upm.edu.my

Abstract: The long-term objective of the present study was to determine the ability of NiZn ferrite nanoparticles to kill cancer cells. NiZn ferrite nanoparticle suspensions were found to have an average hydrodynamic diameter, polydispersity index, and zeta potential of 254.2 ± 29.8 nm, 0.524 ± 0.013, and −60 ± 14 mV, respectively. We showed that NiZn ferrite nanoparticles had selective toxicity towards MCF-7, HepG2, and HT29 cells, with a lesser effect on normal MCF 10A cells. The quantity of *Bcl-2*, *Bax*, *p53*, and *cytochrome C* in the cell lines mentioned above was determined by colorimetric methods in order to clarify the mechanism of action of NiZn ferrite nanoparticles in the killing of cancer cells. Our results indicate that NiZn ferrite nanoparticles promote apoptosis in cancer cells via caspase-3 and caspase-9, downregulation of *Bcl-2*, and upregulation of *Bax* and *p53*, with *cytochrome C* translocation. There was a concomitant collapse of the mitochondrial membrane potential in these cancer cells when treated with NiZn ferrite nanoparticles. This study shows that NiZn ferrite nanoparticles induce glutathione depletion in cancer cells, which results in increased production of reactive oxygen species and eventually, death of cancer cells.

Keywords: NiZn ferrite nanoparticles, cancer cells, reactive oxygen species, cytochrome C, mitochondrial membrane potential, p53

Introduction

Apoptosis is a programmed cellular process involving changes in the expression of distinct genes during cellular death.[1] It is well established that the intrinsic apoptotic pathways occurring through the mitochondrial membrane are regulated by members of the Bcl-2 family,[2] which consists of both repressors (*Bcl-2*, B-cell lymphoma 2 and *Bcl-XL*, B-cell lymphoma-extra large) and inducers (Bax, Bcl-2-associated X and Bak, *Bcl2* [homologous] antagonist/killer) of apoptosis.[3] Among the crucial steps in the intrinsic pathway is an increase in mitochondrial permeability, during which the mitochondrial membrane potential collapses.[4] Bcl-2 proteins appear to play a vital role in preventing the loss of cytochrome C and mitochondrial transmembrane potential during this process.[5] During apoptosis, caspase-9 and Bax proteins migrate to the mitochondria[6] and this is accompanied by DNA fragmentation.[7,8] The Bax proteins trigger the release of cytochrome C in a dose-dependent and time-dependent manner.[9] The consequence of cytochrome C release from the mitochondria is formation of channels in the mitochondrial membrane and subsequent activation of the caspase cascade.[9,10]

Tumor suppressor protein 53 (p53) is a common protein, found in both cancer cells and normal cells,[11] that exhibits potent transcriptional activation of genes, which are

important in cell cycle arrest[12] and apoptosis.[13] It has been suggested that, in cancer cells, p53 induces oxidative stress via enzymes capable of increasing the steady-state level of hydrogen peroxide, a reactive oxygen species.[14] Reactive oxygen species are byproducts generated during mitochondrial electron transport.[15] Prolonged exposure to reactive oxygen species leads to cellular damage,[16] oxidative stress, and DNA fragmentation and, thus, elicits apoptotic mechanisms.[17] Activated oxygen is another reactive oxygen species produced by oxidative stress, which reacts with the double bonds of lipid hydrocarbon in the cell membrane to initiate lipid peroxidation.[18] Thus, measurement of the degree of lipid peroxidation is frequently employed to determine cellular oxidant activity.[19] During lipid peroxidation, malondialdehyde and hydroxyoctadecadienoic acid are produced,[20,21] and both of these compounds are powerful tools in determining oxidative stress.[22,23] Scavenging free radicals and protection of cell viability against toxic oxygen-derived chemical species are facilitated by glutathione.[24,25] In addition, it was suggested that excessive reactive oxygen species facilitates the detachment of cytochrome C and causes dysfunction of the electron-transport chain.[26] This process is necessary for its translocation into the cytoplasm through the mitochondrial pores created by proapoptotic Bcl-2 family proteins such as Bax.[27]

Along these lines, several types of ferrite nanoparticles have a strong potential to be developed into anticancer delivery systems because of the fact that they can be easily internalized into cells[28] to facilitate cancer cell targeting.[29,30] Ni ferrite nanoparticles can destroy the ability of the cancer cell to protect itself against the toxic actions of free radicals by reducing glutathione levels, increasing catalase, superoxide dismutase, and glutathione peroxidase activity, and causing downregulation of the antiapoptotic *Bcl-2* gene.[31]

We have previously determined the magnetization values of NiZn ferrite nanoparticles, showing them to be superparamagnetic at a temperature above the blocking temperature of 300 K in a zero field.[32] As a result of their superparamagnetic behavior, NiZn ferrite nanoparticles now have many potential applications, including in cell imaging[33] and cell therapy.[34] In our previous studies,[35] we have characterized NiZn ferrite nanoparticles and showed them to be toxic to HT29, MCF-7, and HepG2 cells. In the present study, the effects of NiZn ferrite nanoparticles on the generation of reactive oxygen species and their influence on glutathione and lipid peroxidation levels were determined in three cancer cell lines. This study also investigated the mechanism of action of NiZn ferrite nanoparticles, particularly with regard to the induction of cytochrome C release from mitochondria and their influence on antiapoptotic and proapoptotic protein expression.

Materials and methods

Chemicals and preparation of NiZn magnetic nanoparticles

Trypsin-ethylenediaminetetraacetic acid was purchased from Invitrogen (Carlsbad, CA, USA). Dimethylsulfoxide, phosphate-buffered saline, Dulbecco's Modified Eagle's Medium (DMEM), and trypan blue dye were purchased from Sigma-Aldrich (St Louis, MO, USA). NiZn ferrite nanoparticles (chemical formula $Ni_{0.5}Zn_{0.5}Fe_2O_4$) of 98.5% purity were sourced from Nanostructured and Amorphous Materials, Inc. (Garland, TX, USA). The compound was formulated using a simple precipitation technique which utilized the nickel, zinc, and iron nitrates as precursors in a ratio of 0.5:0.5:2.0 following a technique described elsewhere.[32]

Characterization

Powder X-ray diffraction patterns were recorded as previously determined[35] using a Shimadzu XRD-6000 instrument (Shimadzu Corporation, Kyoto, Japan) with CuK_α radiation ($\lambda = 1.5418$ Å) and a dwell time of 4 degrees per minute. Ultraviolet spectra were recorded using a Lambda 900 ultraviolet visible spectrometer (Perkin Elmer, Waltham, MA, USA) with a scan speed of 250 nm per minute. The hydrodynamic size and zeta potential of an NiZn ferrite nanoparticle dispersion (1 µg of NiZn ferrite nanoparticles dispersed in 1 mL of ultradeionized water) were characterized using a ZetaSizer Nano ZS (Malvern Instruments Ltd, Malvern, UK) with dynamic light scattering. In addition, transmission electron microscopy (TEM Model CM12 Philips; Eindhoven, The Netherlands) with an accelerating voltage of 120 kV and a maximum magnification limit of 660 k times, was used to determine the homogeneity of NiZn ferrite nanoparticles.

Cancer cell lines

Three virus-negative human cancer cell lines, ie, breast adenocarcinoma MCF-7 (ATCC® HTB-22™), colorectal adenocarcinoma HT29 (ATCC® HTB-38™), hepatocellular carcinoma HepG2 (ATCC® 77400), and a breast epithelial MCF 10A (ATCC® CRL-10317™) line were obtained from the American Type Culture Collection (Rockville, MD, USA). The cells were cultured and passaged (less than 20 passages) in DMEM (Sigma-Aldrich) as an adherent monolayer of tightly knit epithelial cells.

Trypan blue exclusion assay

To determine the antiproliferative effect of NiZn ferrite nanoparticles, the MCF-7, HepG2, and HT29 cells were first seeded (2×10^4 cells/ml in DMEM) in six-well tissue culture plates. After incubation for 24 hours to allow cell attachment, the exponentially growing cells were exposed to NiZn ferrite nanoparticles at concentrations of 10, 50, 100, and 1000 μg/mL. The plates were then incubated at 37°C in the presence of 5% CO_2 for 12 and 36 hours. After incubation, the medium was aspirated, the plates were washed with cold phosphate-buffered saline to remove dead cells, and replenished with 1 mL of 0.05% (2 mg/mL) trypsin-ethylenediaminetetraacetic acid. The plates were then incubated at 37°C for 10–15 minutes, until the majority of the cells detached as microscopically confirmed. The cells were harvested and the cell suspension was centrifuged at 1,000 rpm for 10 minutes and the supernatant discarded. The 20 μL cell suspension was then mixed with 20 μL of a 0.4% trypan blue solution, the cells were subsequently resuspended, and dye-excluding viable cells were microscopically counted using a hemocytometer chamber.

Lactate dehydrogenase assay

A lactate dehydrogenase release assay was performed to investigate the effect of NiZn ferrite nanoparticles on cell membrane permeability in HepG2, MCF-7, and HT29 cells. The cells were seeded in 96-well culture plates at a density of 2×10^4 cells/well in a 100 μL volume and allowed to grow for 18 hours before treatment. After treatment with 10, 50, 100, and 1000 μg/mL NiZn ferrite nanoparticle suspensions, the plates were incubated for 12 or 36 hours. Forty microliters of supernatant were transferred to a new 96-well to determine lactate dehydrogenase release. The total lactate dehydrogenase was determined in the original plate after the addition of 40 μL of 6% Triton X-100. A 100 μL aliquot of potassium phosphate buffer (0.1 M, pH 7.5) containing 4.6 mM pyruvic acid was mixed with the supernatant using repeated pipetting. Next, 100 μL of the same potassium phosphate buffer containing 0.4 mg/mL reduced β-nicotinamide-adenine dinucleotide was added to the wells. The kinetic changes were read for one minute using an enzyme-linked immunosorbent assay microplate reader at a wavelength of 340 nm. This procedure was repeated with 40 μL of total cell lysate to determine the total lactate dehydrogenase in each well. The percentage of cytotoxicity produced by NiZn ferrite nanoparticles was calculated relative to absorbance (Abs) values for the untreated cells and values resulting from total lysis of cells by Triton X-100 (100% cell kill) according to the formula in Figure 1.[36]

Bcl-2, Bax, p53, and cytochrome C proteins assays

To quantify the p53, Bax, Bcl-2, and cytochrome C proteins in the cells treated with NiZn ferrite nanoparticles, enzyme-linked immunosorbent assay kits (R&D Systems, Minneapolis, MN, USA) were used to determine the change in protein concentration after 12 and 36 hours of exposure to NiZn ferrite nanoparticles according to the manufacturer's instructions; the experiments were conducted as previously described. The absorbance was estimated using a microplate reader, and the results were presented as the relative expression of treated and untreated cells.

Determination of mitochondrial transmembrane potential

The effect of NiZn ferrite nanoparticles on the mitochondrial membrane potential was determined by the quantity of rhodamine 123 efflux; experiments were conducted as previously described. Three microliters of a 5 mg/mL rhodamine solution were incubated with a 1×10^6/mL cell suspension in phosphate-buffered saline. The rhodamine 123 efflux or retention was analyzed using FACSCalibur™ flow cytometry (Becton Dickinson, NJ, USA) and the data were analyzed using CellQuest 3.3 software (Becton Dickinson).

Determination of reactive oxygen species

For determining reactive oxygen species generation, cells treated with NiZn ferrite nanoparticles as previously described were washed with phosphate-buffered saline containing 2′,7′-dichlorofluorescein diacetate. The reactive oxygen species was allowed to oxidize 2′,7′-dichlorofluorescein diacetate to dichlorofluorescein for 10 minutes. After washing, the cells were lysed in buffer (50 mM Tris-HCl, 100 mM NaCl, 1 mM $CaCl_2$, 1 mM $MgCl_2$, 300 mM sucrose,

$$\text{Cytotoxicity (\%)} = [(\text{Abs}_{\text{treated cells}} - \text{Abs}_{\text{untreated cells}}) / (\text{Abs}_{\text{total cells}} - \text{Abs}_{\text{untreated cells}})] \times 100\%$$

Figure 1 Equation to determine percentage of cytotoxicity produced by NiZn ferrite nanoparticles.
Abbreviation: Abs, absorbance at 340 nm.

1% Triton X-100, pH 7.4). The fluorescence of the lysates was determined in a stirred quartz cuvette at 530 nm with an excitation wavelength of 485 nm. The fluorescence intensity of dichlorofluorescein is proportional to the amount of reactive oxygen species formed intracellularly.

Malondialdehyde assay

For determination of malondialdehyde synthesis, the NiZn ferrite nanoparticle-treated cells (performed as previously described) were washed with phosphate-buffered saline, harvested, and homogenized in ice-cold 1.15% KCl. Quantification of malondialdehyde was completed by reacting with thiobarbituric acid and measuring the pink chromophore produced. The data were expressed as thiobarbituric acid-reactive substances.[37]

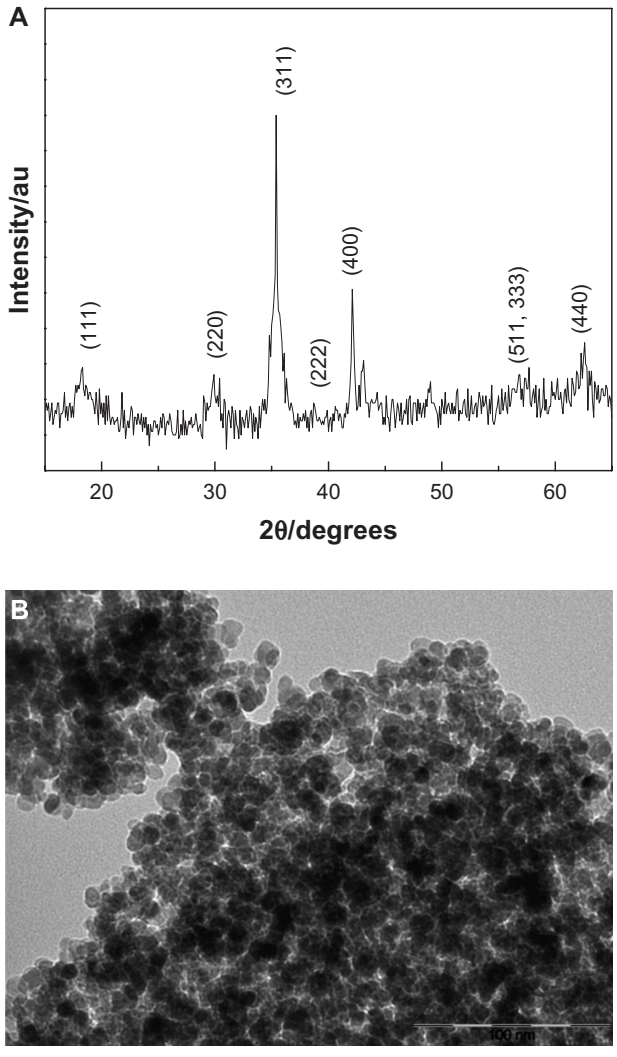

Figure 2 Characterization of NiZn ferrite nanoparticles using X-ray diffractograms (**A**) and transmission electron microscopy (**B**).
Note: Figure 2A reproduced with permission from Dove Medical Press. Al-Qubaisi MS, Rasedee A, Flaifel MH, et al. Cytotoxicity of NiZn ferrite nanoparticles on cancer cells of epithelial origin. *Int J Nanomedicine*. 2013;8:2497–2508.[35]

Glutathione assay

Lastly, the Ellman method[38] was used to estimate the amount of glutathione in NiZn ferrite nanoparticle-treated cancer cells. This method is based on the reaction between the sulfhydryl group of glutathione and 5,5′-dithio-bis-2-nitrobenzoic (DTNB) acid (Ellman reagent) to produce the yellow 5-thio-2-nitrobenzoic (NTB) acid and then measured colorimetrically at 405 nm using UV-vis spectrophotometer. The results were expressed as nmol/mg cells lysate protein.

Statistical analysis

All experiments were completed in triplicate. The data were expressed as the mean ± standard deviation and analyzed using Minitab statistical software (Minitab Inc, State College, PA, USA). Treatment effects were determined using one-way analysis of variance followed by Tukey's post hoc analysis. A value of $P < 0.05$ was considered to be statistically significant unless indicated otherwise.

Results

X-ray diffraction analysis

Figure 2A shows the X-ray diffraction patterns of the NiZn ferrite nanoparticles. The particles have seven characteristic peaks at 2θ = 18.3°, 30.0°, 35.2°, 38.7°, 42.1°, 57.0°, and 62.4°, which can be indexed to the (111), (220), (311), (222), (400), (511, 333), and (440) planes of a cubic cell[39] with (a) lattice parameter value of 8.4 Å. The average crystal grain size was 12 nm, as calculated using the Debye–Scherrer method.

Ultraviolet absorbance analysis

Figure 3 shows the absorption spectrum of NiZn ferrite nanoparticles at room temperature. The maximum ultraviolet absorbance and absorption coefficient were found to be approximately 395 nm and 0.33 cm^{-1}, respectively. The absorbance behavior is a result of the manifold of charge-transfer transitions between O (2p) and mixed ferrites (3d) states, ie, due to the spin-allowed charge-transfer transitions.

Size and zeta potential

The average hydrodynamic diameter, polydispersity index (PDI), and zeta potential for the NiZn ferrite nanoparticle suspensions were 254.2 ± 29.8 nm, 0.524 ± 0.013, and –60 ± 14 mV, respectively, as shown in Figure 4. Transmission electron microscopic image showed the lateral dimension to be 11 nm on average as previously shown.[35] The TEM photograph of pure NiZn ferrite nanoparticles was shown in Figure 2B. It is apparent that NiZn ferrite nanoparticles are approximately

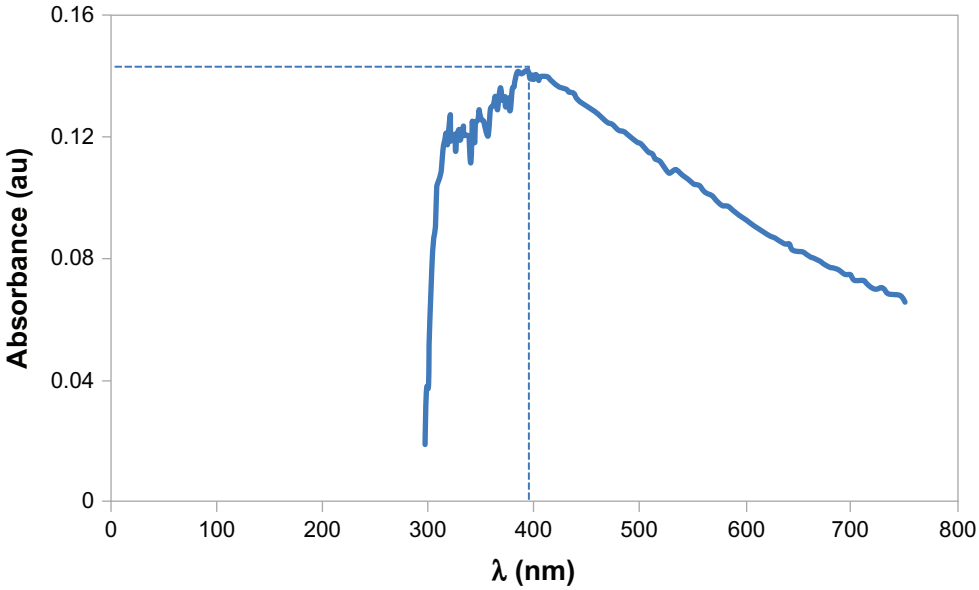

Figure 3 Ultraviolet-visible absorption spectra of NiZn ferrite colloidal nanoparticles in ethanol.

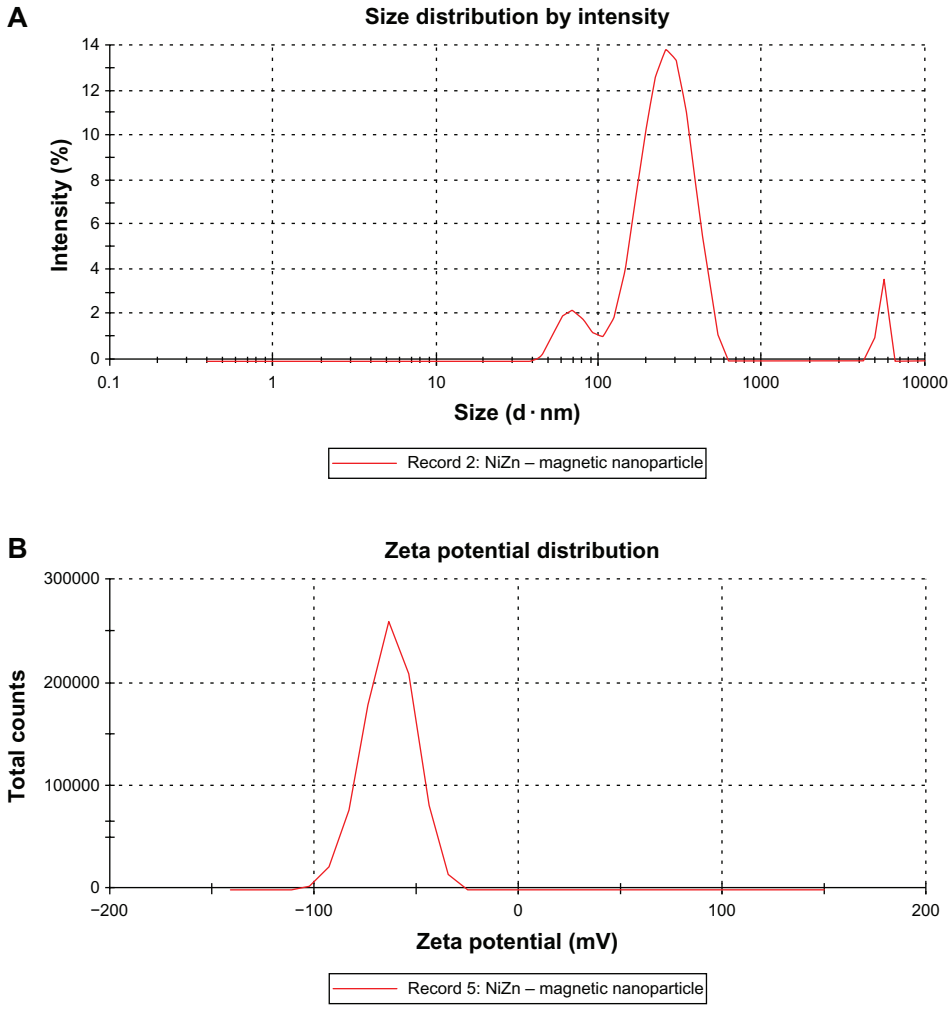

Figure 4 Particle size (**A**) and surface charge (**B**) characterization of NiZn ferrite nanoparticles.

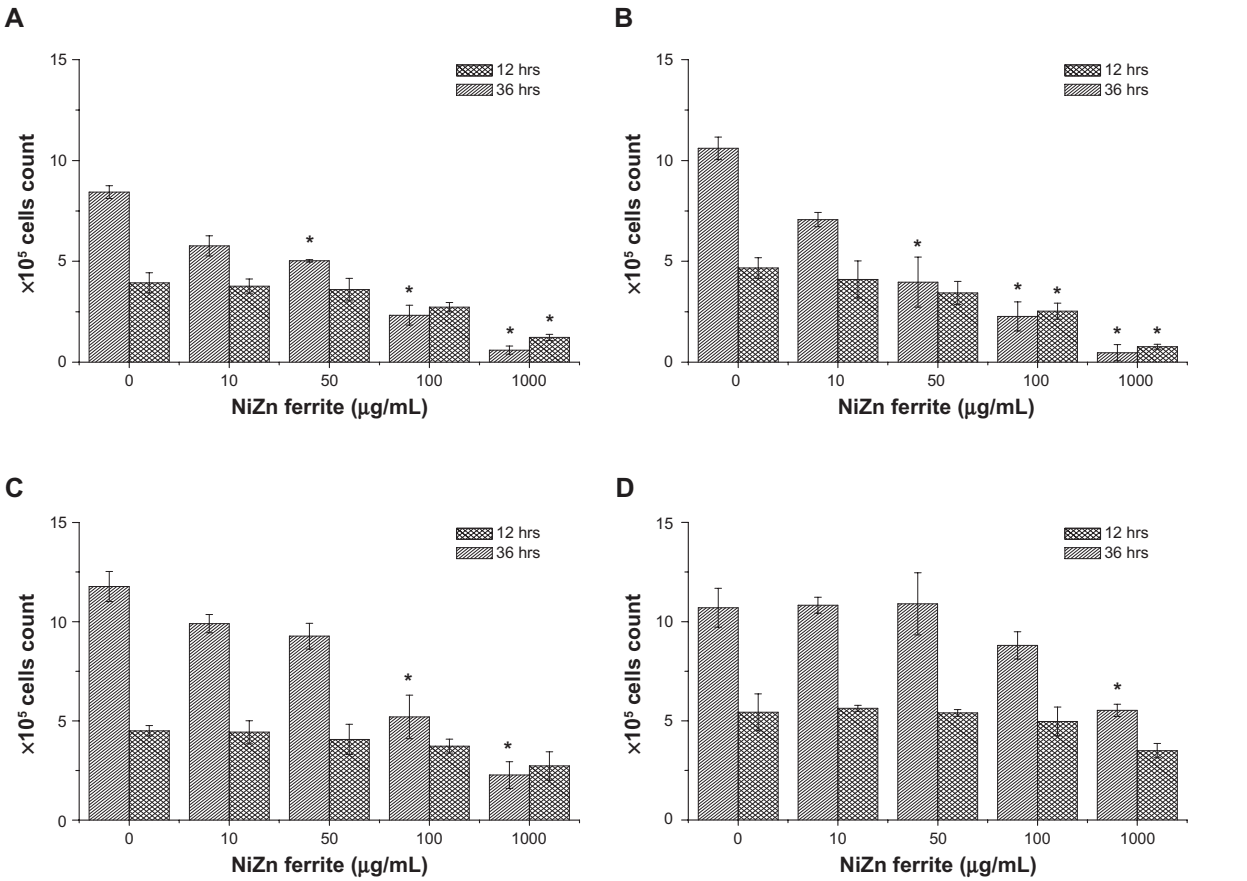

Figure 5 Trypan blue exclusion assay for cell viability of (**A**) HT29, (**B**) HepG2, (**C**) MCF-7, and (**D**) MCF 10A cancer cells after 12 and 36 hours (hrs) of treatment with NiZn ferrite nanoparticles. Mean ± standard deviation (n = 3 wells/treatment). *$P < 0.05$ compared with untreated cells.

spherical in shape with diameter ranging from 10–30 nm. In addition, most of the nanoparticles are agglomerated, and few are detached suggesting the presence of high magnetic-dipole interparticle interactions among the nanoparticles.

Inhibitory effects of NiZn ferrite nanoparticles on cancer cell growth

The antiproliferative activity of NiZn ferrite nanoparticles was determined in cancer cells incubated for 12 and 36 hours at four different concentrations, ie, 10, 50, 100, and 1000 µg/mL. The effect of the nanoparticles on cell proliferation was analyzed using the trypan blue dye exclusion method. The maximal inhibition of all cancer cell lines upon exposure to NiZn ferrite nanoparticles was at 1000 µg/mL after 36 hours of incubation, as shown in Figure 5.

The HepG2 cells were the most sensitive to the antiproliferative effect of NiZn ferrite nanoparticles. Thirty-six hours of exposure to 10 µg/mL NiZn ferrite nanoparticles was enough to decrease the number of viable cells from 10×10^5 cells/mL to 4.0×10^5 cells/mL compared with 10.6×10^5 cells/mL in untreated cells. The percentage survival of HT29 cells treated with 10 µg/mL NiZn nanoparticles was reduced markedly with exposure time to 95% and 68% of untreated cells after 12 and 36 hours, respectively. The MCF-7 cells were less sensitive than the HT29 or HepG2 cells. The number of viable MCF-7 cells treated with a concentration of 10 µg/mL NiZn ferrite nanoparticles for 36 hours was 10.0×10^5 cells/mL while that for untreated cells was 11.8×10^5 cells/mL. The HT29 and HepG2 cells were susceptible to the antiproliferative action of NiZn ferrite nanoparticles. Upon exposure to NiZn ferrite nanoparticles at a concentration of 100 µg/mL for 12 and 36 hours, the number of viable HT29 and HepG2 cells decreased sharply from 69% to 27% and from 54% to 21% of untreated cells, respectively (Figure 5).

Lactate dehydrogenase activity, which is a measure of cell membrane permeability, is another indicator of cell viability. Lactate dehydrogenase activity is measured in the incubation medium of the cell suspension as the enzyme leaks from dead cells which have lost membrane integrity. The toxic effects of NiZn ferrite nanoparticles on the cancer cells were assessed over 12 and 36 hours. NiZn ferrite nanoparticles showed time-dependent and concentration-dependent increases in lactate dehydrogenase release in the tested cancer cells (Figure 6).

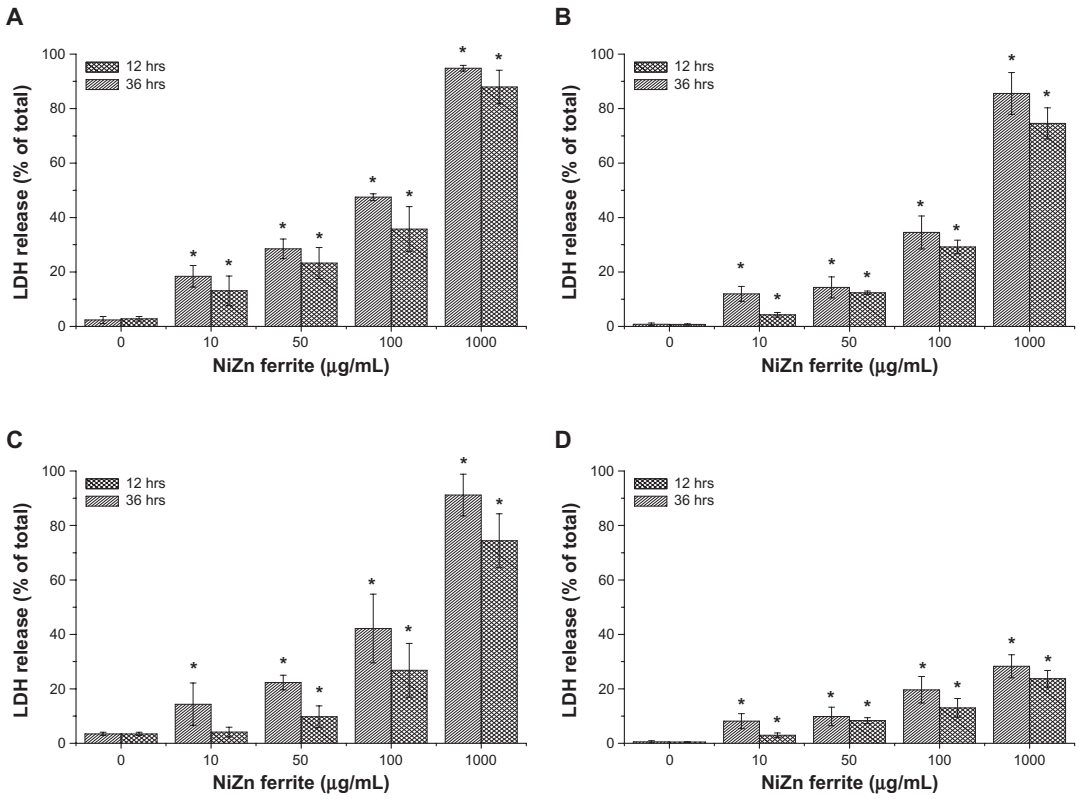

Figure 6 Lactate dehydrogenase (LDH) activity was measured in (**A**) HepG2, (**B**) MCF-7, (**C**) HT29, and (**D**) MCF 10A cancer cells after 12 and 36 hours (hrs) of treatment at 10, 50, 100, and 1000 μg/mL. Data are expressed as a percentage of untreated samples (mean ± standard deviation) of three separate experiments performed in triplicate. Mean ± standard deviation (n = 3 wells/treatment). *$P < 0.05$ compared with untreated cells.

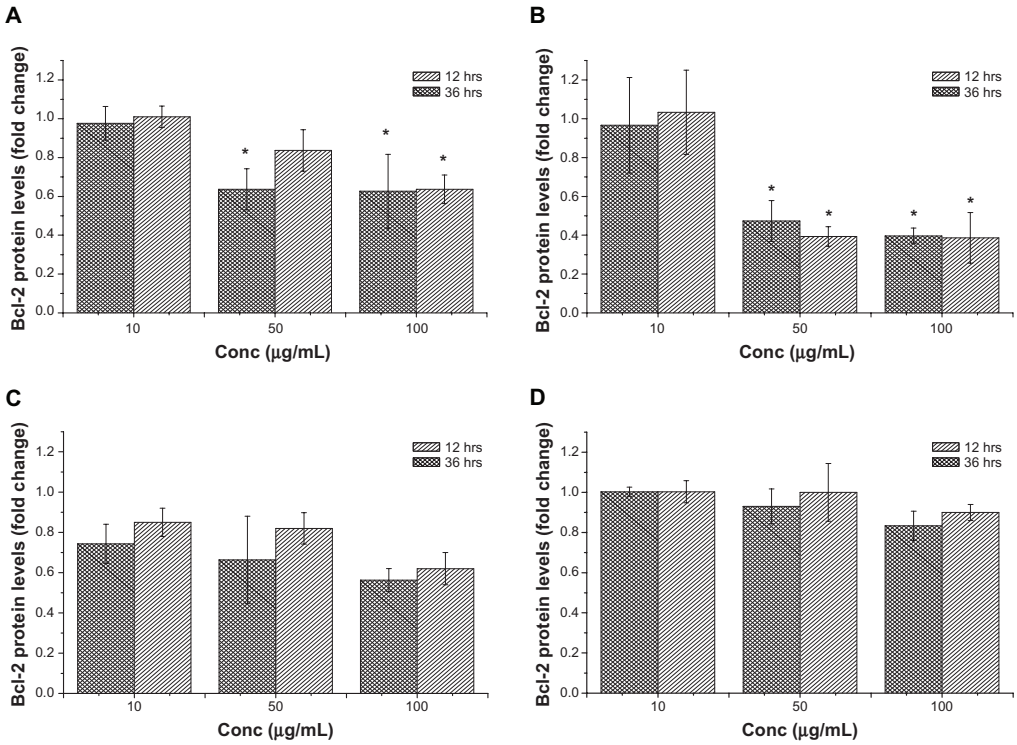

Figure 7 Variations in the demotion of Bcl-2 protein in (**A**) HepG2, (**B**) MCF-7, (**C**) HT29, and (**D**) MCF 10A cells after treatment with NiZn ferrite nanoparticles (10, 50, and 100 μg/mL) for 12 and 36 hours (hrs). The Bcl-2 protein levels are shown as the relative ratios for nanoparticle-treated cells to that of untreated cells. Mean ± standard deviation (n = 3 wells/treatment). *$P < 0.05$ compared with untreated cells.
Abbreviation: Conc, concentation.

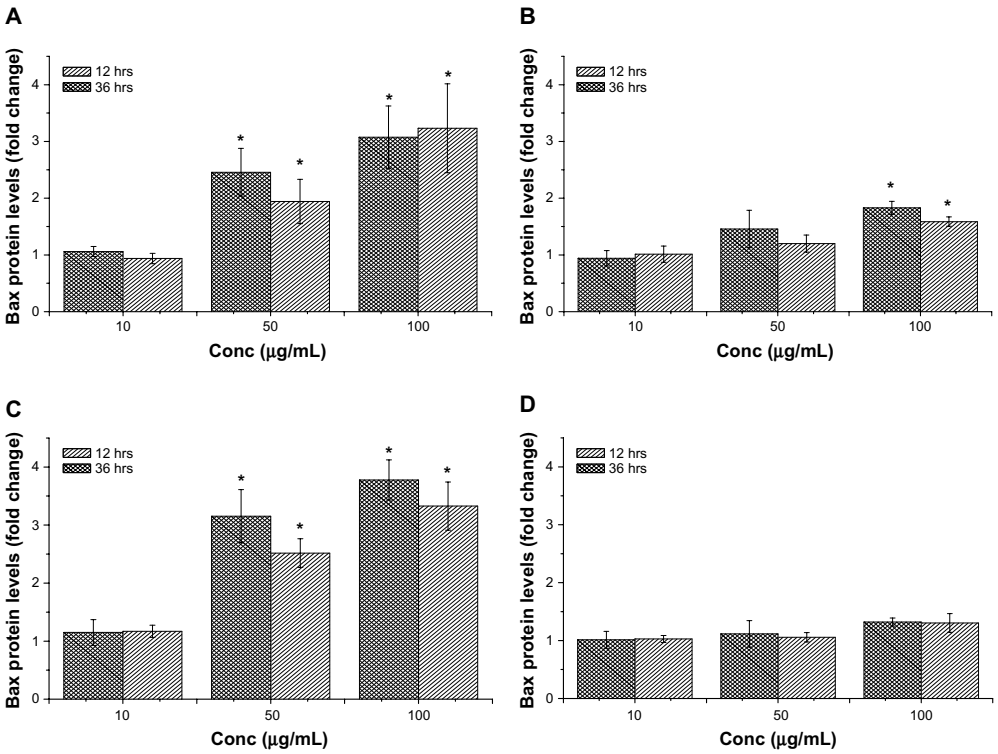

Figure 8 Variations in the elevation of Bax protein in (**A**) HepG2, (**B**) MCF-7, (**C**) HT29, and (**D**) MCF 10A cells after treatment with NiZn ferrite nanoparticles (10, 50, and 100 µg/mL) for 12 and 36 hours (hrs). The Bax protein levels are shown as the relative ratios for nanoparticle-treated cells to that of untreated cells. Mean ± standard deviation (n = 3 wells/treatment). *$P < 0.05$ compared with untreated cells.
Abbreviation: Conc, concentation.

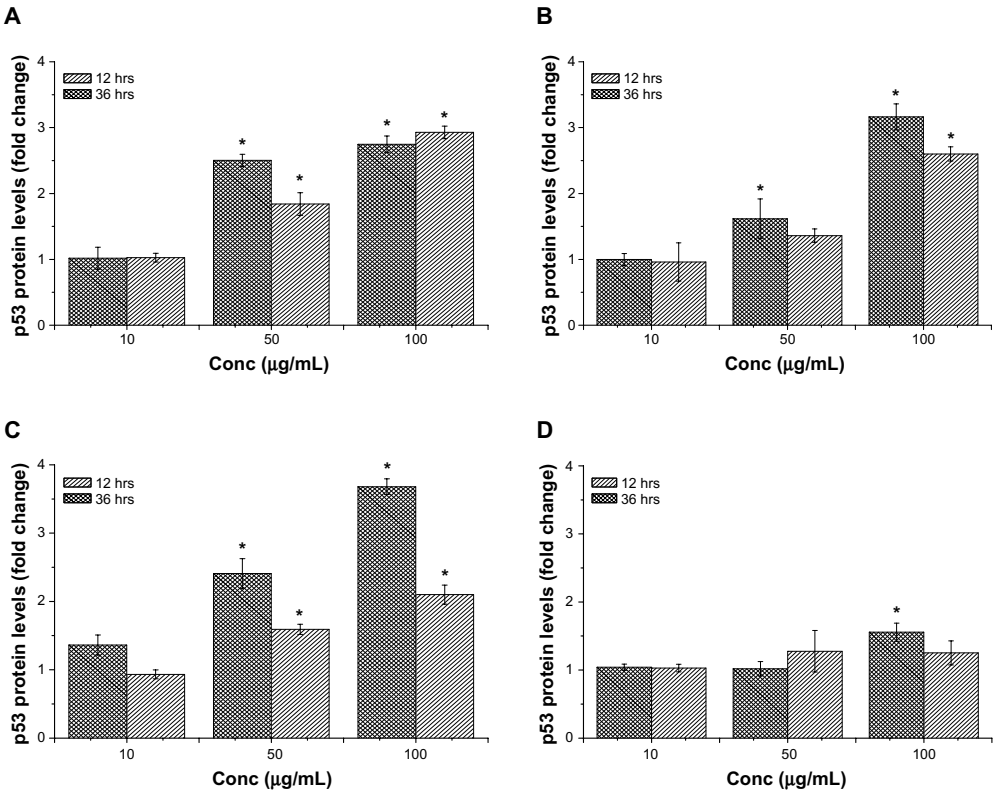

Figure 9 Variations in the elevation of p53 protein in (**A**) HepG2, (**B**) MCF-7, (**C**) HT29, and (**D**) MCF 10A cells after treatment with NiZn ferrite nanoparticles (10, 50, and 100 µg/mL) for 12 and 36 hours (hrs). The p53 protein levels are shown as the relative ratios for nanoparticle-treated cells to that of untreated cells. Mean ± standard deviation (n = 3 wells/treatment). *$P < 0.05$ compared with untreated cells.
Abbreviation: Conc, concentation.

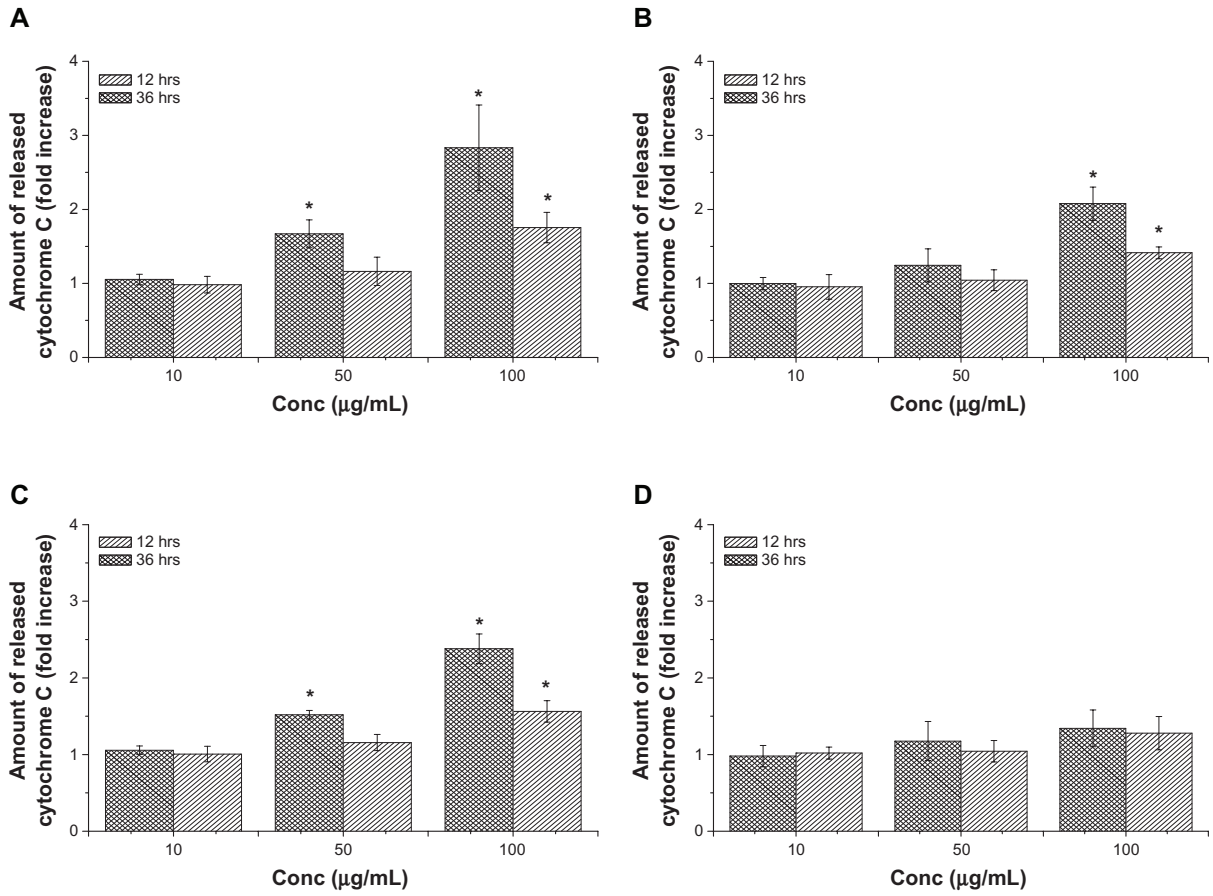

Figure 10 Variations in translocation of cytochrome C protein into the cytosol in (**A**) HepG2, (**B**) MCF-7, (**C**) HT29, and (**D**) MCF 10A cells after treatment with NiZn ferrite nanoparticles (10, 50, and 100 μg/mL) for 12 and 36 hours (hrs). The amount of released cytochrome C is shown as the relative ratio for nanoparticle-treated cells to that of untreated cells. Mean ± SD (n = 3 wells/treatment). *$P < 0.05$ compared with untreated cells.
Abbreviation: Conc, concentation.

The lactate dehydrogenase activity assay indicated that, in the presence of 100 μg/mL NiZn ferrite nanoparticles, 47%, 34%, and 42% loss of cell viability was observed in the HepG2, MCF-7, and HT29 cells, respectively, after 36 hours, whereas exposure to 1000 μg/mL NiZn ferrite nanoparticles caused almost total cell death.

Measurement of Bcl-2, Bax, p53 and cytochrome C proteins

We found that the Bcl-2 protein level reduced by more than 60% in MCF-7 cells, which was three-fold or greater than in the HepG2 (17%) and HT29 (18%) cells after 12 hours of treatment with 50 μg/mL NiZn ferrite nanoparticles compared with untreated cells (Figure 7). The NiZn ferrite nanoparticles gradually downregulated Bcl-2 protein expression in the HepG2 and HT29 cells during the 36-hour treatment, becoming significant by the end of the treatment period. In contrast with Bcl-2, Bax protein expression increased by 2–3-fold in HepG2 and HT29 cells treated with 50 μg/mL nanoparticles compared with untreated cells after 12 hours (Figure 8). However, in the NiZn ferrite nanoparticle-treated MCF-7 cells, the increase in Bax protein expression was not significant. We also determined the effect of NiZn ferrite nanoparticles on p53 protein expression using the enzyme-linked immunosorbent assay method. As shown in Figure 9, significant differences in p53 protein expression were found between untreated HT29 and HepG2 cells and those treated with 50 and 100 μg/mL NiZn ferrite nanoparticles for 36 hours. In the MCF-7 cells, significant p53 expression was only observed after treatment with 100 μg/mL NiZn ferrite nanoparticles for 36 hours. Cytochrome C release is a marker for mitochondria-related apoptosis.[40] Cancer cells treated with NiZn ferrite nanoparticles exhibited a concomitant increase in cytochrome C release in a time-dependent and concentration-dependent manner (Figure 10).

Mitochondrial transmembrane potential

We elucidated the effect of NiZn ferrite nanoparticles on mitochondrial membrane potential ($\Delta\Psi m$) using rhodamine 123 efflux, because apoptosis triggers a collapse of the mitochondrial membrane potential ($\Delta\Psi m$). Although

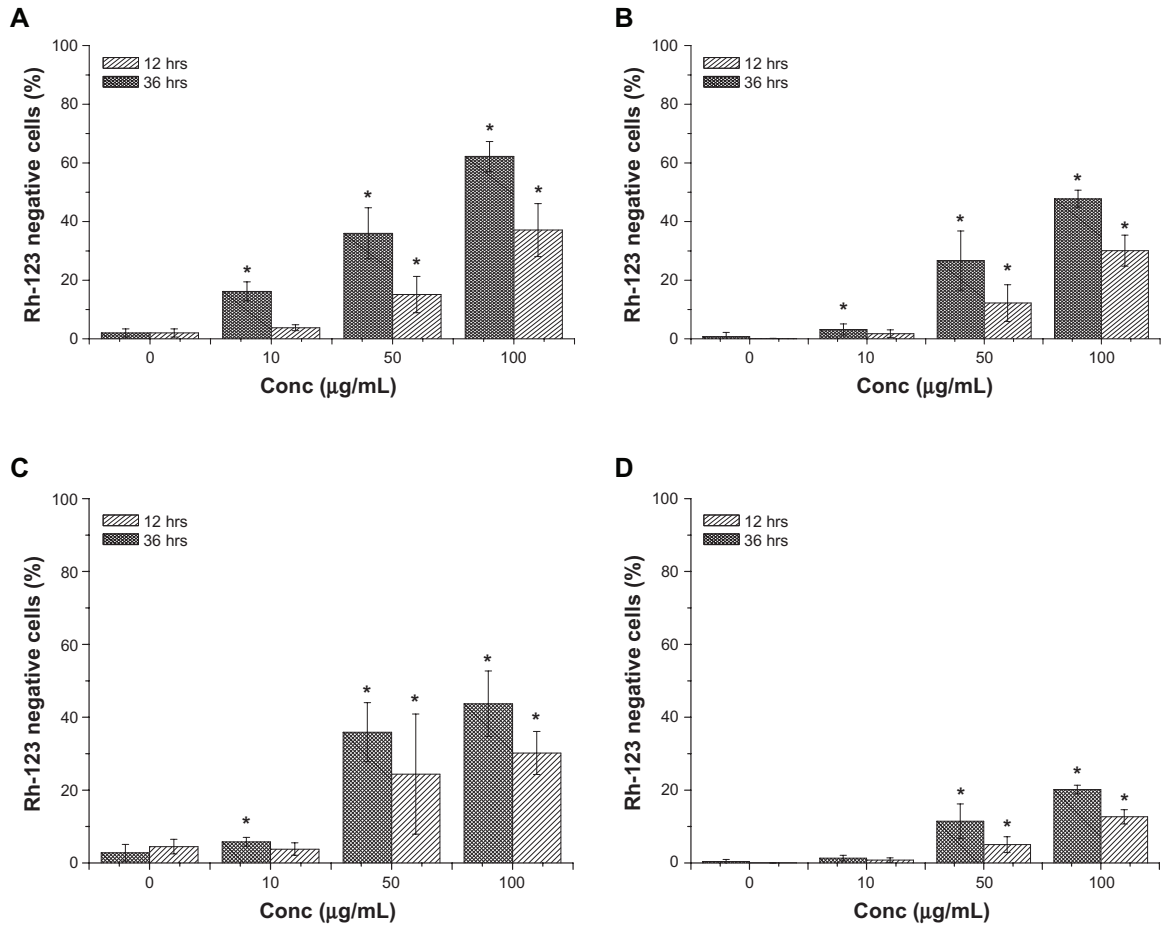

Figure 11 NiZn ferrite nanoparticles induced loss of mitochondrial transmembrane potential. The mitochondrial transmembrane potential was measured by flow cytometry using rhodamine 123 dye. Exposure of (**A**) HepG2, (**B**) MCF-7, (**C**) HT29, and (**D**) MCF 10A cells to NiZn ferrite nanoparticles (10, 50, and 100 µg/mL) for 12 and 36 hours (hrs) decreased the mitochondrial transmembrane potential. Mean ± standard deviation (n = 3 wells/treatment). *$P < 0.05$ compared with untreated cells.
Abbreviations: Conc, concentation; Rh-123, rhodamine 123.

rhodamine 123-negative cells at 12 hours were equally distributed between untreated cells and cells treated with 10 µg/mL NiZn ferrite nanoparticles (Figure 11), at 36 hours the percentage of cells with rhodamine 123 efflux was significantly lower for untreated cells than for treated cells. The highest rhodamine retention (62%) occurred in HepG2 cells treated with 100 µg/mL NiZn ferrite nanoparticles (Figure 11).

Glutathione

Glutathione concentration was determined to assess the effect of NiZn ferrite nanoparticles on cellular metabolic function. When we examined the changes in glutathione levels in HepG2, HT29, and MCF-7 cells in the presence of 50 µg/mL NiZn ferrite nanoparticles for 36 hours, the number of glutathione-depleted cells increased by approximately 48%, 42%, and 43% compared with untreated cells, respectively. In all cancer cells, the relative reduction in glutathione concentrations was similar after treatment with 100 µg/mL NiZn ferrite nanoparticles at 12 and 36 hours (Figure 12).

Malondialdehyde

Lipid peroxidation is a reliable and useful indicator of oxidant stress in cells treated with toxicants.[41] The effect of NiZn ferrite nanoparticles on cancer cell lipid peroxidation is shown in Figure 13. The malondialdehyde levels increased in a time-dependent and concentration-dependent manner. The treatment of HepG2, MCF-7, and HT29 cells with 10 µg/mL NiZn ferrite nanoparticles for 36 hours was associated with increases in malondialdehyde levels from 2.3, 1.9, and 2.3 nM/mg protein to 5.6, 3.5, and 4.0 nM/mg protein, respectively. Similarly, the treatment of HepG2, MCF-7, and HT29 cells with 50 µg/mL NiZn ferrite nanoparticles increased malondialdehyde levels from 6, 4.6, and 7.8 nM/mg protein at 12 hours to 10.6, 6.1, and 9.0 nM/mg protein at 36 hours, respectively.

Reactive oxygen species

Dichlorofluorescein fluorescence was used to identify intracellular mitochondrial reactive oxygen species generation in NiZn ferrite nanoparticle-treated cells. Reactive oxygen

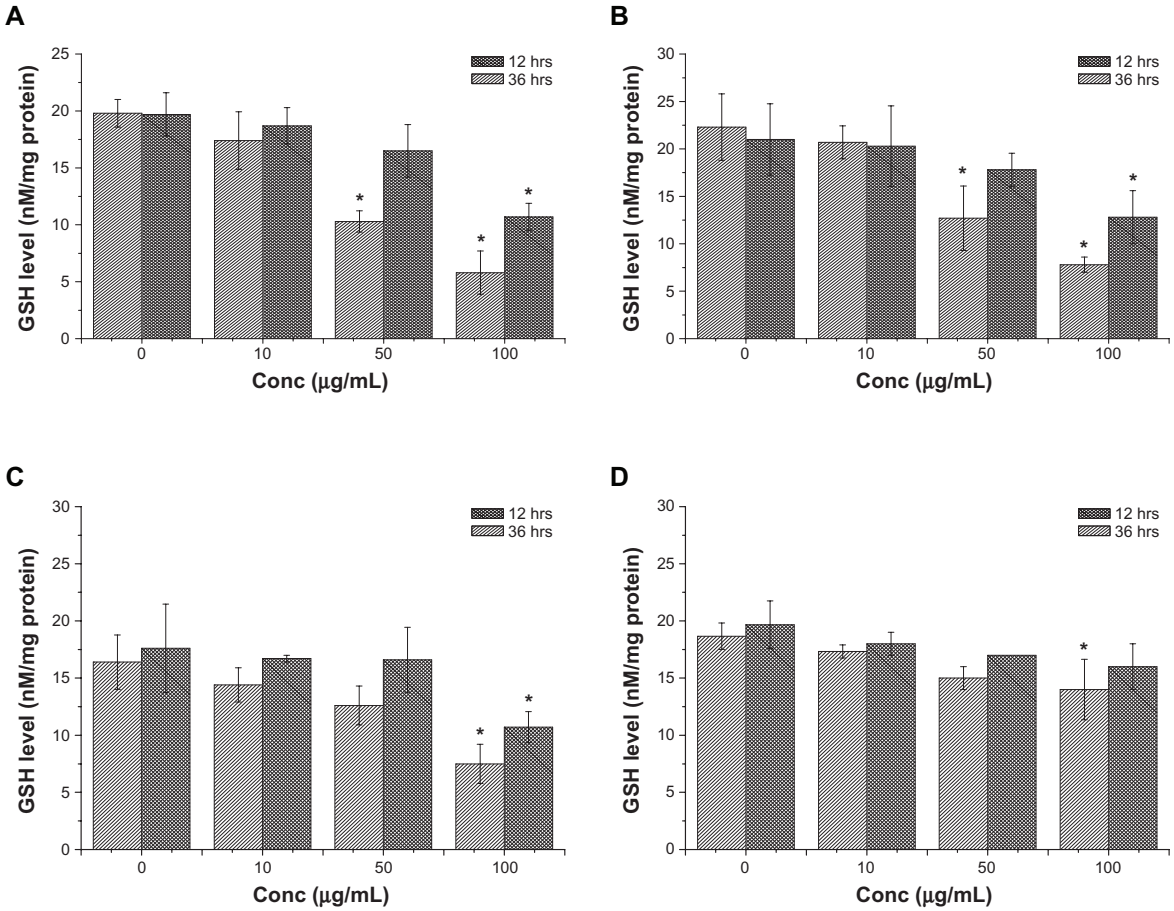

Figure 12 Time course of glutathione (GSH) depletion caused by nanoparticle (10, 50, and 100 µg/mL) exposure in (**A**) HepG2, (**B**) MCF-7, (**C**) HT29, and (**D**) MCF 10A cells. The NiZn ferrite nanoaprticles-treated cells were lysed by sulfosalicylic acid and the samples were centrifuged at 10,000 × g for 5 minutes. Aliquot of 1 mL of the supernatants was added to 2 mL of Ellman's reagent and the absorbance was recorded at 405 nm after 5 minutes. Mean ± standard deviation (n = 3 times per treatment). *$P < 0.05$ compared with untreated cells.
Abbreviations: Conc, concentation; hrs, hours.

species production in the three cancer cell lines treated with 100 µg/mL NiZn ferrite nanoparticles was significantly higher than in untreated cells (Figure 14). At a dose of 50 µg/mL, NiZn ferrite nanoparticles generated a substantial increase in fluorescence intensity of reactive oxygen species in the HT29 and HepG2 cells by approximately 2–3-fold (relative to untreated) after 36 hours. In similarly treated MCF-7 cells, production of reactive oxygen species was not so substantial. The fluorescence intensity after 36 hours of treatment with 10 µg/mL NiZn ferrite nanoparticles did not increase significantly in any of the cancer cell lines (Figure 14).

Discussion

Size analysis showed that the NiZn ferrite nanoparticles have hydrodynamic diameters that are much larger than those shown by transmission electron microscopy.[35] Although this may suggest that NiZn ferrite nanoparticles tend to aggregate in deionized and double-distilled water, their high zeta potential of –60 mV indicates that these nanoparticles have good electrostatic repulsion characteristics and are very stable. At this zeta potential, the NiZn ferrite nanoparticles would repel particle aggregation in suspensions for long-term stability.[42] Thus, the nanoparticles do agglomerate, and specifically, this agglomeration may result in immune system clearance before the particles get to the cancer cells. Immune system clearance of the nanoparticles, either due to the agglomeration or that they are not coated with polyethylene glycol or any entity that would keep macrophages from clearing the nanoparticles requires further characterization assays and investigation. Further, in a previous study, we showed that NiZn ferrite nanoparticles do not remain magnetized in the magnetic field.[32] This phenomenon, termed superparamagnetism, offers advantages to the NiZn ferrite nanoparticles by reducing the tendency for particle aggregation.[32] The absorption spectrum is one of the most useful tools to determine the charge-transfer transitions between different atomic states. As compared with previous studies, the higher energy absorption peak centered around 395 nm (3.14 eV) confirmed the manifold of charge-transfer transitions between O (2p) and mixed ferrite (3d) states.[43–46]

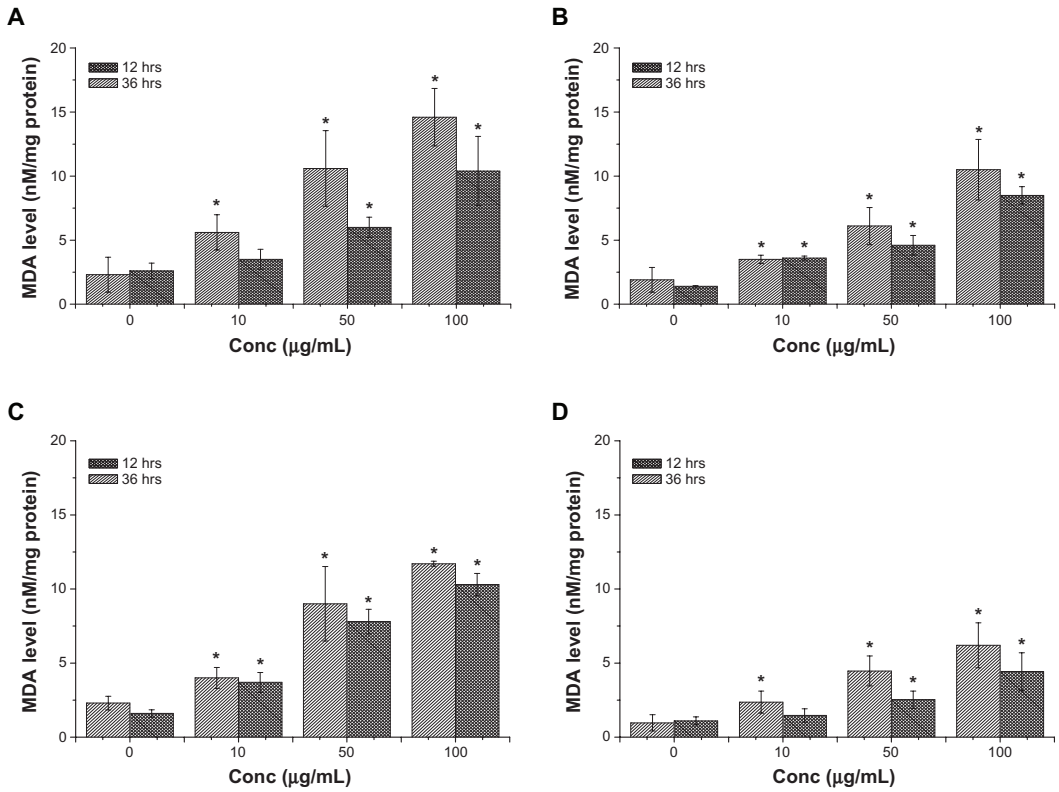

Figure 13 Effect of NiZn ferrite nanoparticle dose on malondialdehyde (MDA) production in (**A**) HepG2, (**B**) MCF-7, (**C**) HT29, and (**D**) MCF 10A cell lines. Cells were exposed for 12 and 36 hours (hrs) to the indicated concentrations of nanoparticles. After changing the medium, the cells were allowed to grow for 24 hours. Malondialdehyde was then assayed in the cell pellets by the thiobarbituric acid reaction. Mean ± standard deviation (n = 3 wells/treatment). *$P < 0.05$ compared with untreated cells.
Abbreviation: Conc, concentation.

Leakage of lactate dehydrogenase is due to the loss of nicotinamide-adenine dinucleotide from oxidation to NAD^+ and conversion of pyruvate to lactate.[47] Leakage of lactate dehydrogenase is an indicator of loss of cell viability. As supported by lactate dehydrogenase results, NiZn ferrite nanoparticles inhibited cell cancer cell proliferation in a time-dependent and concentration-dependent manner, with less harm done to normal MCF 10A cells. This observation is consistent with that shown using MTT and BrdU assays in our earlier study.[35] NiZn ferrite nanoparticles reduced the mitochondrial membrane potential by increasing its permeability in cancer cells. At a 10 µg/mL NiZn ferrite nanoparticle concentration, MCF-7 cells seemed to be resistant to treatment while HepG2 cells were sensitive. This difference in susceptibility can be attributed to the difference between cancer cells in the basal activity of mitochondrial organelles and antioxidant enzymes. Increasing the treatment dose of NiZn ferrite nanoparticles to 100 µg/mL disrupted the mitochondrial integrity, resulting in high leakage of lactate dehydrogenase.

The Bcl-2 family members regulate mitochondrial membrane permeability. Accumulation of Bax in the outer layer of the mitochondria will cause permeability through the formation of transition pores, resulting in release of cytochrome C and ultimately triggering mitochondrial-dependent apoptosis.[48] The level of Bax and p53 expression in cancer cells treated with NiZn ferrite nanoparticles appears to increase with the inhibition of proliferation of HepG2 and HT29 cells. This is consistent with the idea that a decrease in malignant potential is caused by the induction of apoptosis via increased expression of apoptosis inducers.

Loss of mitochondrial membrane potential, which is considered to be the most important feature of the induction of the intrinsic apoptotic pathway, was determined by rhodamine 123 staining. Our results showed a significant decrease in mitochondrial transmembrane potential in HepG2 cells treated with 10 µg/mL NiZn ferrite nanoparticles. That is reflected in a loss of the ability of the cell to accumulate the cationic fluorochrome rhodamine 123 dye, which in turn caused an early time-dependent release of cytochrome C into the cytoplasm. Although rhodamine 123-negative cells were approximately equally distributed between untreated MCF-7 cells and cells treated with 10 µg/mL NiZn ferrite nanoparticles after 12 hours, the percentage of cells with rhodamine 123 efflux was significantly lower in untreated cells than those similarly treated for 36 hours. This finding

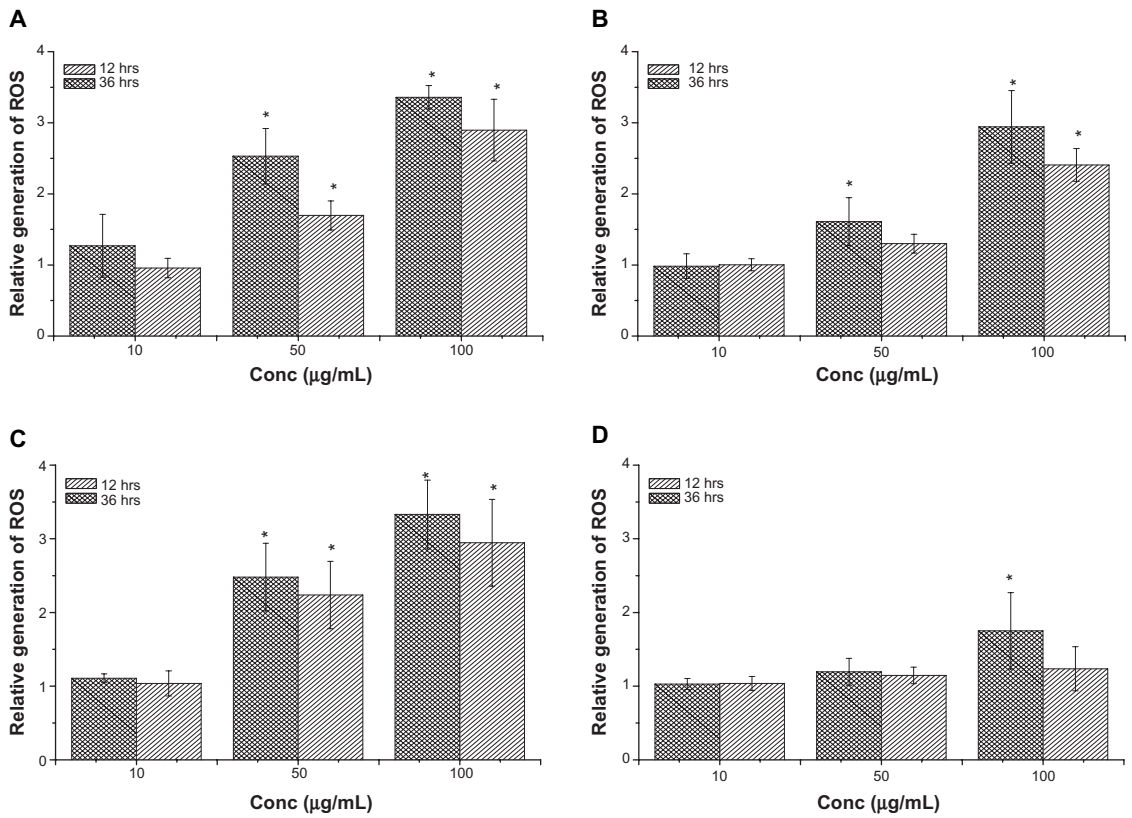

Figure 14 Reactive oxygen species (ROS) generation in vitro in (**A**) HepG2, (**B**) MCF-7, (**C**) HT29, and (**D**) MCF 10a cells treated with NiZn ferrite nanoparticles. Relative fluorescence intensity of sample versus control was calculated. Mean ± standard deviation (n = 3 wells/treatment). *$P < 0.05$ compared with untreated cells.
Abbreviations: Conc, concentation; hrs, hours.

suggests that NiZn ferrite nanoparticles induced apoptosis in cancer cells via the mitochondrial pathway.

The current study also showed that translocation of cytoplasmic Bax to the mitochondrial membrane at low-dose NiZn ferrite treatment in HepG2 and HT29 cells and at a high dose in MCF-7 cells was a key initiating step in apoptosis. The results suggest that the mitochondrial membrane permeability of the cancer cells treated with NiZn ferrite nanoparticles occurred through reduction of Bcl-2 activity and an increase in Bax and p53 activity. The net effect is the death of cancer cells through the activation of caspase-3 mediated by caspase-9, given that induction of apoptosis by ferrite nanoparticles is attributable to their ability to increase the expression of proapoptotic genes, such as caspase-3, caspase-8, and caspase-9 genes.[49] A schematic representation of the proposed apoptotic mechanism of cancer cells due to NiZn ferrite nanoparticles was shown in Figure 15.

Leakage of cytochrome C from the mitochondria into the cytoplasm, increased production of reactive oxygen species, and depletion of cellular glutathione are associated with apoptosis of cancer cells. The reactive oxygen species produced from cancer cells treated with NiZn ferrite nanoparticles also promoted apoptosis by triggering pathways involving mitochondrial release of cytochrome C and activation of caspases. Intracellular reactive oxygen species may target cellular membrane lipids, proteins, and DNA, causing oxidative injury. As a consequence of the accumulation of reactive oxygen species and depletion of glutathione, treated cells may develop mitochondrial dysfunction with subsequent release of cytochrome C, which leads to loss of viability.[50] In our study, glutathione levels were considerably reduced in the HepG2 and MCF-7 cells and slightly reduced in HT29 cells treated with 50 g/mL NiZn ferrite nanoparticles for 12 hours. By 36 hours, glutathione was further depleted, reaching a value approximately 25% lower than that in untreated HT29 cells. This suggests that NiZn ferrite nanoparticles also caused cancer cell death through oxidative stress and DNA fragmentation. NiZn ferrite nanoparticles triggered lipid peroxidation, which was accompanied by the production of reactive oxygen species. In fact, the increased production of reactive oxygen species in cancer cells is also the consequence of glutathione depletion, particularly after 12 hours of exposure to 100 μg/mL and 36 hours of exposure to 50 and 100 μg/mL NiZn ferrite nanoparticles. Further

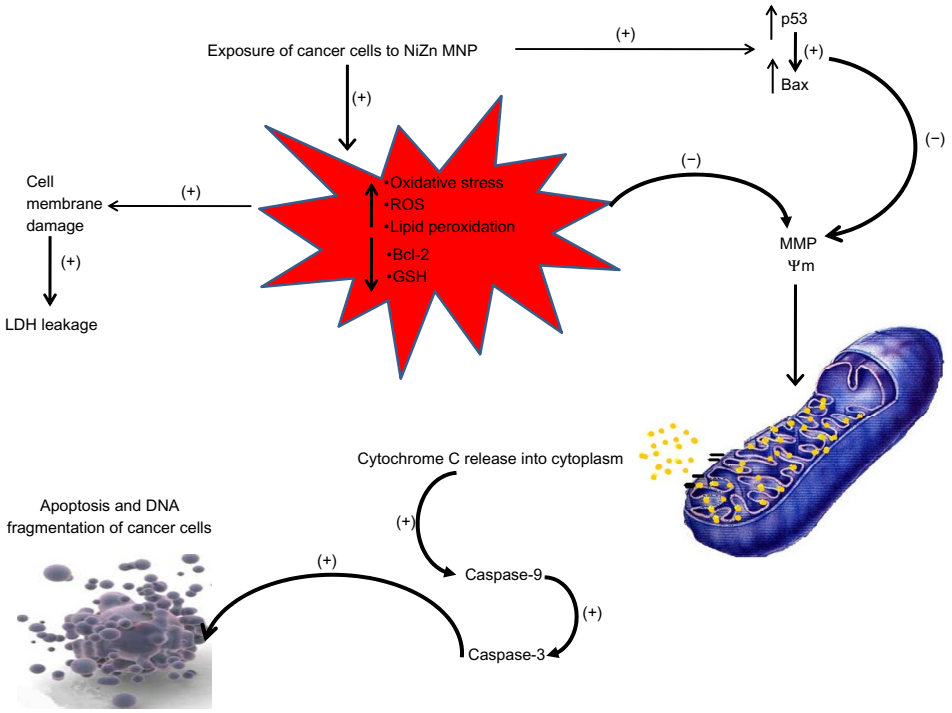

Figure 15 Schematic representation of the response of cancer cells to the exposure to NiZn ferrite nanoparticles.
Notes: As shown, treatment of cancer cells with NiZn ferrite nanoparticles increased both lipid peroxidation production and generation of reactive oxygen species (ROS) associated with the decrease of glutathione (GSH) and downregulation of Bcl-2 which in turn increased oxidative stress in the mitochondria. The oxidative stress in the mitochondrial membrane leads to the release of cytochrome C into the cytoplasm. Moreover, the oxidative stress in the cells induced cell membrane damage which increased outflow of lactate dehydrogenase (LDH) to extracellular space. The increase in p53 and Bax together with the previous biochemical events eventually results in lowering of the mitochondrial membrane potential (MMP) (by increasing the mitochondrial membrane permeability). All of these biological processes facilitate the translocation of cytochrome C from the mitochondrial intermembrane space to the cytoplasm. The released cytochrome C will complex with Apf-1 and caspase-9 to form an apoptosome. Apoptosomes then activate caspase-3 and then subsequently activates other caspases in the cytoplasm, which triggers cell death and DNA fragmentation of cancer cells.

studies are required to elucidate the fate of NiZn ferrite nanoparticles after cancer cell death, whether the detoxifying machinery of normal cells can reduce the toxic load of nickel, and if there are any toxicity concerns associated with their application.

Conclusion

The present study shows that NiZn ferrite nanoparticles induced apoptosis in cancer cells of epithelial origin via the caspase-3-dependent and caspase-9-dependent mitochondrial signaling pathway. NiZn ferrite nanoparticles inhibited Bcl-2, which plays an important role in countering the proapoptotic effects of Bax overexpression. NiZn ferrite nanoparticles can also elicit apoptosis principally through activation of the p53 tumor suppressor protein. The cytotoxic effect of NiZn ferrite nanoparticles was not only due to increasing cell membrane permeability, but also as a result of the induction of oxidative stress via glutathione depletion. These results unequivocally show that there is a link between NiZn ferrite nanoparticle-induced lipid peroxidation and sensitivity to nanoparticles, and this should be investigated further for potential synergistic effects between NiZn ferrite nanoparticles and chemotherapeutics to enhance the efficacy of cancer treatment.

Disclosure

The authors report no conflicts of interest in this work.

References

1. Elmore S. Apoptosis: a review of programmed cell death. *Toxicol Pathol*. 2007;35(4):495–516.
2. Youle RJ, Strasser A. The BCL-2 protein family: opposing activities that mediate cell death. *Nat Rev Mol Cell Biol*. 2008;9(1):47–59.
3. Rodriguez JM, Glozak MA, Ma Y, Cress WD. Bok, Bcl-2-related ovarian killer, is cell cycle-regulated and sensitizes to stress-induced apoptosis. *J Biol Chem*. 2006;281(32):22729–22735.
4. Tomitaka A, Yamada T, Takemura Y. Magnetic nanoparticle hyperthermia using Pluronic-coated Fe3O4 nanoparticles: an in vitro study. *J Nanomater*. 2012;2012:4.
5. Chipuk JE, Green DR. How do BCL-2 proteins induce mitochondrial outer membrane permeabilization? *Trends Cell Biol*. 2008;18(4):157–164.
6. Wei MC, Zong WX, Cheng EH, et al. Proapoptotic BAX and BAK: a requisite gateway to mitochondrial dysfunction and death. *Sci Signal*. 2001;292(5517):727–730.
7. Yang J, Liu X, Bhalla K, et al. Prevention of apoptosis by Bcl-2: release of cytochrome c from mitochondria blocked. *Science*. 1997;275(5303):1129–1132.

8. Susin SA, Lorenzo HK, Zamzami N, et al. Molecular characterization of mitochondrial apoptosis-inducing factor. *Nature*. 1999;397(6718):441–446.
9. Sharpe JC, Arnoult D, Youle RJ. Control of mitochondrial permeability by Bcl-2 family members. *Biochim Biophys Acta*. 2004;1644(2): 107–113.
10. Reed JC. Double identity for proteins of the Bcl-2 family. *Nature*. 1997;387(6635):773–776.
11. Kuerbitz SJ, Plunkett BS, Walsh WV, Kastan MB. Wild-type p53 is a cell cycle checkpoint determinant following irradiation. *Proc Natl Acad Sci U S A*. 1992;89(16):7491–7495.
12. Agarwal ML, Agarwal A, Taylor WR, Stark GR. p53 controls both the G2/M and the G1 cell cycle checkpoints and mediates reversible growth arrest in human fibroblasts. *Proc Natl Acad Sci U S A*. 1995;92(18):8493–8497.
13. Lowe SW, Ruley HE, Jacks T, Housman DE. p53-dependent apoptosis modulates the cytotoxicity of anticancer agents. *Cell*. 1993;74(6):957–967.
14. Migliaccio E, Giorgio M, Mele S, et al. The p66 shc adaptor protein controls oxidative stress response and life span in mammals. *Nature*. 1999;402(6759):309–313.
15. Liu Y, Fiskum G, Schubert D. Generation of reactive oxygen species by the mitochondrial electron transport chain. *J Neurochem*. 2002;80(5):780–787.
16. Hensley K, Robinson KA, Gabbita SP, Salsman S, Floyd RA. Reactive oxygen species, cell signaling, and cell injury. *Free Radic Biol Med*. 2000;28(10):1456–1462.
17. Jacobson MD. Reactive oxygen species and programmed cell death. *Trends Biochem Sci*. 1996;21(3):83–86.
18. Gutteridge J. Lipid peroxidation and antioxidants as biomarkers of tissue damage. *Clin Chem*. 1995;41(12):1819–1828.
19. Halliwell B, Chirico S. Lipid peroxidation: its mechanism, measurement, and significance. *Am J Clin Nutr*. 1993;57(5):715S–724S.
20. Jira W, Spiteller G, Carson W, Schramm A. Strong increase in hydroxy fatty acids derived from linoleic acid in human low density lipoproteins of atherosclerotic patients. *Chem Phys Lipids*. 1998;91(1):1–11.
21. Niki E. Lipid peroxidation: physiological levels and dual biological effects. *Free Radic Biol Med*. 2009;47(5):469–484.
22. Butterfield DA, Lauderback CM. Lipid peroxidation and protein oxidation in Alzheimer's disease brain: potential causes and consequences involving amyloid β-peptide-associated free radical oxidative stress. *Free Radic Biol Med*. 2002;32(11):1050–1060.
23. Markesbery WR. Oxidative stress hypothesis in Alzheimer's disease. *Free Radic Biol Med*. 1997;23(1):134–137.
24. Fang YZ, Yang S, Wu G. Free radicals, antioxidants, and nutrition. *Nutrition*. 2002;18(10):872–879.
25. Robertson RP, Harmon J, Tran PO, Tanaka Y, Takahashi H. Glucose toxicity in β-cells: type 2 diabetes, good radicals gone bad, and the glutathione connection. *Diabetes*. 2003;52(3):581–587.
26. Ow YP, Green DR, Hao Z, Mak TW. Cytochrome c: functions beyond respiration. *Nat Rev Mol Cell Biol*. 2008;9(7):532–542.
27. Desagher S, Martinou JC. Mitochondria as the central control point of apoptosis. *Trends Cell Biol*. 2000;10(9):369–377.
28. Villanueva A, Cañete M, Roca AG, et al. The influence of surface functionalization on the enhanced internalization of magnetic nanoparticles in cancer cells. *Nanotechnology*. 2009;20(11):115103.
29. Johannsen M, Gneveckow U, Eckelt L, et al. Clinical hyperthermia of prostate cancer using magnetic nanoparticles: presentation of a new interstitial technique. *Int J Hyperthermia*. 2005;21(7):637–647.
30. Ito A, Shinkai M, Honda H, Kobayashi T. Medical application of functionalized magnetic nanoparticles. *J Biosci Bioeng*. 2005;100(1): 1–11.
31. Ahamed M, Akhtar MJ, Siddiqui MA, et al. Oxidative stress mediated apoptosis induced by nickel ferrite nanoparticles in cultured A549 cells. *Toxicology*. 2011;283(2):101–108.
32. Flaifel MH, Ahmad SH, Abdullah MH, Al-Asbahi BA. NiZn ferrite filled thermoplastic natural rubber nanocomposites: effect of low temperature on their magnetic behaviour. *Cryogenics*. 2012;52(10):523–529.
33. Jendelová P, Herynek V, DeCroos J, et al. Imaging the fate of implanted bone marrow stromal cells labeled with superparamagnetic nanoparticles. *Magn Reson Med*. 2003;50(4):767–776.
34. McCarthy JR, Weissleder R. Multifunctional magnetic nanoparticles for targeted imaging and therapy. *Adv Drug Deliv Rev*. 2008;60(11):1241–1251.
35. Al-Qubaisi MS, Rasedee A, Flaifel MH, et al. Cytotoxicity of NiZn ferrite nanoparticles on cancer cells of epithelial origin. *Int J Nanomedicine*. 2013;8:2497–2508.
36. Crawford KW, Bowen WD. Sigma-2 receptor agonists activate a novel apoptotic pathway and potentiate antineoplastic drugs in breast tumor cell lines. *Cancer Res*. 2002;62(1):313–322.
37. Hodges DM, DeLong JM, Forney CF, Prange RK. Improving the thiobarbituric acid-reactive-substances assay for estimating lipid peroxidation in plant tissues containing anthocyanin and other interfering compounds. *Planta*. 1999;207(4):604–611.
38. Owens C, Belcher R. A colorimetric micro-method for the determination of glutathione. *Biochem J*. 1965;94(3):705–711.
39. Sreeja V, Vijayanand S, Deka S, Joy P. Magnetic and Mössbauer spectroscopic studies of NiZn ferrite nanoparticles synthesized by a combustion method. *Hyperfine Interact*. 2008;183(1–3):99–107.
40. Chua CC, Liu X, Gao J, Hamdy RC, Chua BH. Multiple actions of pifithrin-α on doxorubicin-induced apoptosis in rat myoblastic H9c2 cells. *Am J Physiol Heart Circ Physiol*. 2006;290(6):H2606–H2613.
41. Muniz JF, McCauley L, Scherer J, et al. Biomarkers of oxidative stress and DNA damage in agricultural workers: a pilot study. *Toxicol Appl Pharmacol*. 2008;227(1):97–107.
42. Yallapu MM, Othman SF, Curtis ET, Gupta BK, Jaggi M, Chauhan SC. Multi-functional magnetic nanoparticles for magnetic resonance imaging and cancer therapy. *Biomaterials*. 2011;32(7):1890–1905.
43. Wang X, Li D, Cui T, Kharel P, Liu W, Zhang Z. Magnetic and optical properties of multiferroic GdMnO3 nanoparticles. *J Appl Phys*. 2010;107:09B510.
44. Lv H, Ma L, Zeng P, Ke D, Peng T. Synthesis of floriated ZnFe2O4 with porous nanorod structures and its photocatalytic hydrogen production under visible light. *J Mater Chem*. 2010;20(18):3665–3672.
45. Harish K, Bhojya Naik H, Kumar PP, Viswanath R. Remarkable optical and photocatalytic properties of solar light active Nd substituted Ni ferrite catalysts: for environment protection. *ACS Sustainable Chemistry and Engineering*. 2013.
46. Wang X, Li D, Cui T, Kharel P, Liu W, Zhang Z. Magnetic and optical properties of multiferroic $GdMnO_3$ nanoparticles. *J Appl Phys*. 2010;107(9):09B510.
47. Al-Qubaisi M, Rozita R, Yeap SK, Omar AR, Ali AM, Alitheen NB. Selective cytotoxicity of goniothalamin against hepatoblastoma HepG2 cells. *Molecules*. 2011;16(4):2944–2959.
48. Platoshyn O, Zhang S, McDaniel SS, Yuan JX. Cytochrome c activates K+ channels before inducing apoptosis. *Am J Physiol Cell Physiol*. 2002;283(4):C1298–C1305.
49. Fang L, Chen B, Liu S, et al. Synergistic effect of a combination of nanoparticulate Fe3O4 and gambogic acid on phosphatidylinositol 3-kinase/Akt/Bad pathway of LOVO cells. *Int J Nanomedicine*. 2012;7:4109–4118.
50. Kane DJ, Sarafian TA, Anton R, et al. Bcl-2 inhibition of neural death: decreased generation of reactive oxygen species. *Science*. 1993;262(5137):1274–1277.